

## **Title: Aromatic and antiaromatic ring currents in a molecular nanoring**

*Authors: Martin D. Peeks, Timothy D. W. Claridge & Harry L. Anderson\**

**Aromatic and antiaromatic molecules exhibit ring currents around their perimeters<sup>1,2</sup>. Similar persistent currents are observed in metal rings, when the coherence length of the electrons is longer than the circumference of the ring<sup>3,4</sup>. The relationship between these quantum mechanical phenomena is poorly understood, partly because they are studied in different size regimes: the largest aromatic molecules have diameters of about 1 nm, whereas persistent currents are found in rings with diameters of 20–1000 nm. It is not clear whether aromaticity and antiaromaticity are confined to small molecules, or whether the necessary quantum coherence can be achieved in large macrocycles. Here we show, using <sup>1</sup>H NMR spectroscopy and density functional theory, that a six-porphyrin nanoring template complex *c*-P6·T6, with a diameter of 2.4 nm, is antiaromatic in its 4+ oxidation state and aromatic in its 6+ oxidation state. These species have circuits of 80 and 78  $\pi$  electrons, respectively, and they are the largest aromatic and antiaromatic systems yet reported. The antiaromatic state has a huge paramagnetic susceptibility, despite having no unpaired electrons. This work demonstrates that a global ring current can be promoted in a macrocycle by adjusting its oxidation state to suppress the local ring currents of its components. The discovery of ring currents around a molecule with a circumference of 7.5 nm, at room temperature, shows that quantum coherence can persist in surprisingly large molecular frameworks, and implies that it will be possible to exploit quantum interference effects, such as Aharonov-Bohm oscillations, in molecular electronic devices.**

Chemists have been fascinated by aromatic compounds ever since Faraday isolated benzene in the 1820s, and aromaticity has become an important concept for understanding molecules with delocalised electronic structures<sup>1,2</sup>. Hückel's rule predicts that a molecule will be aromatic or antiaromatic if it has a delocalised circuit of  $[4n + 2]$  or  $[4n]$  electrons, respectively, where  $n$  is an integer. These ideas were developed by studying cyclic hydrocarbons known as annulenes, with the general formula  $C_mH_m$  (where  $m$  is even)<sup>5</sup>, and the prototypical aromatic and antiaromatic molecules are benzene ( $C_6H_6$ ) and cyclobutadiene ( $C_4H_4$ ), respectively.

The most characteristic feature of aromatic and antiaromatic molecules is their ability to sustain an induced ring current in a magnetic field. Molecular ring currents are quantum mechanical phenomena and their main manifestation is induced magnetisation<sup>6</sup>. In aromatic molecules, the direction of the ring current is such as to generate a magnetic field that opposes the external field inside the ring (a 'diatropic' current), while ring currents in antiaromatic molecules flow in the reverse direction ('paratropic')<sup>7</sup>. These ring currents give rise to diagnostic NMR chemical shifts<sup>7</sup>, and are accompanied by diamagnetic and paramagnetic susceptibility exaltations, for aromatic and antiaromatic molecules respectively, and large out-of-plane magnetic anisotropies<sup>8</sup>. The persistent currents observed in metal and semiconductor rings resemble aromatic ring currents<sup>3,4</sup>, and in direct analogy to Hückel's rule, the direction of the persistent current depends on the number of electrons in the system<sup>9</sup>. Persistent currents in non-molecular rings switch direction as a function of the magnetic flux passing through the ring, so that they can be changed from diatropic ('aromatic') to paratropic ('antiaromatic') simply by changing the strength of the external magnetic field. The magnetic field required for one such Aharonov-Bohm oscillation is inversely proportional to the area of the ring and absurdly high fields would be needed to test this effect in small molecules (*e.g.* a benzene molecule, with a

diameter of 0.3 nm, would require a field of  $6 \times 10^4$  T for one cycle). Understanding the connection between aromaticity and the persistent currents in mesoscopic rings provides a strong motivation for investigating ring currents in molecules of an intermediate size<sup>10</sup>.

Studies on annulenes have led to the conclusion that aromaticity decreases with increasing ring size and vanishes for systems with more than about 30  $\pi$  electrons (corresponding to a diameter of around 1.3 nm)<sup>11,12</sup>, but it seems likely that aromaticity can be preserved in larger systems if geometrical disorder is suppressed<sup>13</sup>. The previous record for the largest aromatic molecule is held by a  $50\pi$  dodecaphyrin with a diameter of about 1.3 nm<sup>14</sup>. The dication of [8]cycloparaphenylene ([8]CPP,  $30\pi$ , diameter 1.1 nm) is also aromatic<sup>15</sup>. We recently reported the synthesis of  $\pi$ -conjugated macrocycles consisting of 5–50 porphyrin units, with diameters of 2–20 nm, (**c-PN**,  $N = 5$ –50, Fig. 1), as well as the corresponding linear oligomers **l-PN**<sup>16–18</sup>. The **c-PN** rings might all be expected to exhibit diatropic or paratropic ring currents around the whole nanoring because they all have circumferential circuits of  $[4n + 2]$  or  $[4n]$   $\pi$  electrons (*e.g.* **c-P6**  $84\pi$ ; **c-P7**  $98\pi$ ), yet, as in [8]CPP, the neutral molecules exhibit no signs of global aromaticity or antiaromaticity. Here we demonstrate that aromaticity and antiaromaticity are exhibited in different oxidation states.

Density functional theory (DFT) calculations of the nucleus independent chemical shift (NICS)<sup>19</sup> at the centre of the ring (Table S2) provide insights into the behaviour of the **c-P6** nanoring cations. The NICS(0)<sub>zz</sub> indicate aromaticity for the 6+ oxidation state, while 0 (neutral) and 12+ are non-aromatic, and 4+ is antiaromatic. The NICS(0)<sub>iso</sub> calculated on a grid in the *xy* plane (the plane of the six Zn atoms) for **c-P6**, **c-P6**<sup>4+</sup>, **c-P6**<sup>6+</sup> and **c-P6**<sup>12+</sup> clearly demonstrates the nature of the ring current in each oxidation state (Fig. 2 and SI Fig. S8). For the neutral **c-P6**, the ring current effects are localised above and below the plane of each porphyrin unit, with no net

global ring current (Fig. 2a). This result is in stark contrast to **c-P6<sup>4+</sup>**, where the NICS is positive (NMR deshielding) inside the macrocycle, and negative (shielding) outside, characteristic of paratropicity (Fig. 2b). This effect is reversed in the aromatic **c-P6<sup>6+</sup>**, with shielding inside the macrocycle, and deshielding outside (Fig. 2c). The NICS(0)<sub>iso</sub> grid for the 12+ (SI Fig. S8) shows local porphyrin antiaromaticity, with no global aromaticity, consistent with six local 16 $\pi$  antiaromatic porphyrin ring-currents. For the 6+, we also calculated NICS<sub>zz</sub> in the orthogonal xz and yz planes (SI Fig. S6 and S7), showing that the shielding anisotropy of the nanoring extends as a double cone above and below the plane of the ring. Models of the anisotropy of the induced current density (ACID)<sup>20</sup> support the conclusions from NICS, demonstrating a coherent current ACID isosurface for **c-P6<sup>4+</sup>** and **c-P6<sup>6+</sup>** (with paratropic and diatropic current directions, respectively; current vectors shown in SI Fig. S9), in contrast to an interrupted isosurface for **c-P6** and **c-P6<sup>12+</sup>** (Fig. 2d–f and SI Fig. S9). Many antiaromatic systems, including cyclobutadiene, undergo a Jahn-Teller distortion to favour a low-symmetry conformation, and this effect is evident in **c-P6<sup>4+</sup>**. The geometries of **c-P6** and **c-P6<sup>6+</sup>** converge in *D*<sub>6h</sub> symmetry whereas **c-P6<sup>4+</sup>** has *C*<sub>1</sub> symmetry with an elliptical flattening factor of *f* = 0.049 (defined as 1 – *b/a*, where *a* and *b* are the major and minor radii of the Zn6 ellipse). **c-P6<sup>12+</sup>** also has *C*<sub>1</sub> symmetry but in this case there is almost no ellipticity (*f* < 10<sup>–3</sup>).

The nanoring cations can be generated in solution by chemical or electrochemical oxidation. Square-wave voltammetry (SWV) of **c-P6·T6** reveals six reversible porphyrin-centred oxidations in a first manifold, at +0.1–0.7 V (vs. Fc/Fc<sup>+</sup>) (Fig. 3; see SI Fig. S13 for spectroelectrochemistry). The second manifold comprises a single six-electron oxidation to generate **c-P6·T6<sup>12+</sup>**, in which each porphyrin unit is in its 2+ oxidation state. All of the oxidation states are accessible by titration with tris(2,4-dibromophenyl)aminium hexafluoroantimonate

(DIBAHAF,  $E_{\text{red}} = 1.14$  V), and specific oxidation states can be targeted with diacetylferrocenium hexafluoroantimonate (diAcFc,  $E_{\text{red}} = 0.50$  V), tris(4-bromophenyl)aminium hexafluoroantimonate (BAHAF,  $E_{\text{red}} = 0.70$  V) and thianthrenium hexafluoroantimonate (Thn,  $E_{\text{red}} = 0.86$  V) (all *vs.* Fc/Fc<sup>+</sup>, Fig. 3, SI Fig. S1 for structures)<sup>21</sup>. Titration of DIBAHAF into a solution of **c-P6·T6** at 223 K in CD<sub>2</sub>Cl<sub>2</sub> gives a sequence of three resolved <sup>1</sup>H NMR spectra (Fig. 4), assigned to the 4+ (red-brown solution), 6+ (burgundy solution) and 12+ (grey/black solution) oxidation states (*vide infra*). There is no further change in the NMR spectrum upon addition of excess DIBAHAF: the 12+ state is the endpoint. Identical spectra are obtained using AgSbF<sub>6</sub>/I<sub>2</sub> (4:1 or 2:1) as the oxidant. Intermediates with odd numbers of electrons are not observed during these titrations, presumably because their spectra are extremely broad. The spectrum for the 2+ oxidation state (*i.e.* after addition of 2 eq. oxidant) is also too broad to observe, indicating that **c-P6·T6**<sup>2+</sup> is open-shell and paramagnetic. We confirmed the oxidation state of the first two resolved products (4+ and 6+) by single-point oxidations with diAcFc (4+), BAHAF (6+) and Thn (6+). These single-point oxidation NMR spectra are reproducible in the presence of supporting electrolyte (0.1 M Bu<sub>4</sub>NPF<sub>6</sub>).

Before presenting the NMR evidence for global nanoring (anti)aromaticity in the 4+ and 6+ oxidation states, we calibrate discussion of the <sup>1</sup>H NMR spectra on the well-studied<sup>22</sup> neutral **c-P6·T6**. The porphyrin β-pyrrole protons resonate at the characteristic chemical shifts for neutral porphyrins (*a*: 9.56 ppm, *b*: 8.75 ppm, Fig. 4a; Table S3). Rotation of *meso*-aryl groups is slow on the NMR timescale (see SI for details), so that the inner and outer *ortho* protons (*o* and *o'*) and trihexylsilyl resonances (THS and THS') can be confidently distinguished. A global aromatic ring current would shield the inner protons (*o'* and THS') and deshield the outer protons (*o* and THS) causing large differences in chemical shift ( $\Delta\delta = \delta_{\text{inner}} - \delta_{\text{outer}}$ ). It is observed that these

signals give small chemical shift differences ( $\Delta\delta_{o/o'} = 0.26$  ppm;  $\Delta\delta_{THS/THS'} = 0.14$  ppm) in the neutral ring, implying that there is no global ring current. The ring current of each aromatic  $18\pi$  porphyrin unit is apparent from the  $^1\text{H}$  chemical shifts of the template protons  $\alpha$ ,  $\beta$ ,  $\gamma$  and  $\delta$ , which are shielded by the porphyrin; the shielding is attenuated with increasing distance from the porphyrin:  $\alpha \gg \beta > \gamma > \delta$  (Fig. 4a and Table S4).

The  $^1\text{H}$  NMR spectrum of **c-P6·T6<sup>4+</sup>** is very broad (Fig. 4b), precluding detailed assignment of the resonances. However, a clear splitting of the THS groups is apparent in the aliphatic region (SI Fig. S22). The less shielded set of THS resonances shows multiple NOEs to resonances at high chemical shift (8–24 ppm), and is thus assigned to the inner THS' group (SI Fig. S19). The large positive  $\Delta\delta_{THS/THS'}$  (3.45 ppm) implies a strong macrocyclic paratropic ring current. Antiaromaticity is further supported by an extremely high paramagnetic susceptibility exaltation for **c-P6·T6<sup>4+</sup>** measured by Evans' NMR method and corroborated by DFT calculations;  $\chi_{mol}$  (experimental) = 21,000 ppm cm<sup>3</sup> mol<sup>-1</sup> ( $\mu_{\text{eff}} = 6.5 \mu_{\text{B}}$ ),  $\chi_{mol}$  (calc.) = 68,000 ppm cm<sup>3</sup> mol<sup>-1</sup>, ( $\mu_{\text{eff}} = 11.5 \mu_{\text{B}}$ ), compared to  $\chi_{mol} = 1480$  ppm cm<sup>3</sup> mol<sup>-1</sup> ( $\mu_{\text{eff}} = 1.7 \mu_{\text{B}}$ ) expected for a single unpaired electron (all units c.g.s.; see SI Fig. S4, Table S2). Despite many predictions of paramagnetism in closed-shell antiaromatic compounds<sup>23</sup>, to the best of our knowledge, this is the first time that the effect has been observed experimentally. Experimental studies of other antiaromatic systems have found a reduction in the diamagnetism rather than outright paramagnetism<sup>8</sup>. 'Giant orbital paramagnetism' has been predicted, but not observed, for carbon-based nanostructures such as carbon nanotube tori<sup>24</sup>.

In contrast to **c-P6·T6<sup>4+</sup>**, the NMR spectrum of **c-P6·T6<sup>6+</sup>** is well resolved and fully assigned by 2D techniques (see SI Figs. S20, S23–24). A large  $\Delta\delta$  is observed between the *o/o'* (−1.87 ppm) and THS/THS' (−0.70 ppm) resonances. NOEs to the template were used to assign the

inner *vs.* outer resonances. The inner *o'* and THS' are more shielded than their external counterparts (negative  $\Delta\delta$ ) in **c-P6·T6<sup>6+</sup>**, confirming the presence of a global diatropic ring current. The template protons  $\alpha$ – $\delta$  are all nearly equally shielded with respect to unbound **T6** (Table S4), revealing a uniform shielding effect within the macrocycle, as predicted by the NICS grids (Fig. 2c), and indicating the absence of local porphyrin aromaticity.

The <sup>1</sup>H NMR spectrum of **c-P6·T6<sup>12+</sup>** is well resolved and was fully characterised by 2D NMR techniques (SI Figs S21, S25 and S26). In **c-P6·T6<sup>12+</sup>**, every porphyrin unit is in the antiaromatic 16 $\pi$  dicationic oxidation state<sup>25</sup>. The antiaromatic porphyrin centres deshield the template protons (with respect to unbound template, Table S4); the extent of deshielding decreases with distance from the porphyrin plane,  $\alpha \gg \beta > \gamma > \delta$  (Fig. 4d). This behaviour is entirely local to the 16 $\pi$  porphyrin unit, as demonstrated by the similarity between the <sup>1</sup>H NMR spectra of the porphyrin monomer **l-P1<sup>2+</sup>**, dimer **l-P2<sup>4+</sup>**, tetramer **l-P4<sup>8+</sup>**, and cyclic oligomers **c-P6·T6<sup>12+</sup>**, **c-P6<sup>12+</sup>**, **c-P8·T8<sup>16+</sup>**, **c-P10<sup>20+</sup>**, **c-P11<sup>22+</sup>** and **c-P12<sup>24+</sup>** (all recorded in the presence of excess DIBAHA<sub>F</sub>; SI Fig. S10 and S11). Comparison of the SWV of **l-P1** and **l-P2** shows that the first oxidation wave of **l-P1** is split upon oligomer homologation, while the second oxidation wave is not split (SI Fig. S12). This lack of electronic communication is reflected in the highest occupied molecular orbital (HOMO) of **l-P2<sup>4+</sup>**, corresponding to the Gouterman a<sub>1u</sub> orbital<sup>26</sup>, which exhibits no density at the porphyrin *meso* positions (SI Figs. S14). In contrast, the HOMOs of neutral oligomers exhibit high density at the *meso* positions (Gouterman a<sub>2u</sub>), leading to strong electronic communication in *meso-meso* linked porphyrin oligomers<sup>27</sup>.

The <sup>1</sup>H NMR spectra of **c-P6<sup>6+</sup>** and **c-P6<sup>12+</sup>** with no bound template are very similar to those of the template complexes, except for the absence of template signals (SI Fig. S15 and S16). We were unable to observe a <sup>1</sup>H NMR spectrum of **c-P6<sup>4+</sup>** without the bound template, and the

conformational lock provided by the template seems to be essential for creating a well-defined antiaromatic system. Neutral butadiyne-linked porphyrin oligomers have a very low barrier to torsional rotation about the alkyne axis<sup>28</sup> and fast exchange occurs between the *ortho* (*o* and *o'*) resonances in **c-P6**, even at low temperature, due to this free rotation. In contrast, the *o* and *o'* resonances are split at low temperature for **c-P6**<sup>6+</sup> ( $T < 263$  K; SI Fig. S17) and **c-P6**<sup>12+</sup> ( $T < 243$  K; SI Fig. S18), indicating increased conjugation between porphyrin subunits in these oxidation states. EXSY NMR experiments at 213 K revealed  $\Delta G^\ddagger$  of  $49.5 \pm 0.4$  kJ mol<sup>-1</sup> and  $42.6 \pm 0.4$  kJ mol<sup>-1</sup> for 6+ and 12+ respectively (see SI text, Figs S2 and S3, and Table S1, for details). The **c-P6**<sup>6+</sup> hexacation is aromatic with or without the bound **T6** template, but the template has two important roles in this system: it holds the nanoring in a regular geometry, resulting in sharper NMR spectra, and it provides a set of protons to probe the magnetic effects of the ring current at well-defined positions inside the nanoring.

## References:

1. T. M. Krygowski, M. K. Cyrański, Z. Czarnocki, G. Häfeli, A. R. Katritzky, Aromaticity: a theoretical concept of immense practical importance. *Tetrahedron* **56**, 1783–1796 (2000).
2. R. Gleiter, G. Haberhauer, *Aromaticity and Other Conjugation Effects* (Wiley-VCH 2012).
3. A. C. Bleszynski-Jayich, W. E. Shanks, B. Peaudecerf, E. Ginossar, F. von Oppen, L. Glazman, J. G. E. Harris, Persistent currents in normal metal rings. *Science* **326**, 272–275 (2009).



4. A. Lorke, R. J. Luyken, A. O. Govorov, J. P. Kotthaus, J. M. Garcia, P. M. Petroff, Spectroscopy of nanoscopic semiconductor rings. *Phys. Rev. Lett.* **84**, 2223–2226 (2000).
5. E. L. Sitler, C. A. Johnson II, M. M. Haley, Renaissance of annulene chemistry. *Chem. Rev.* **106**, 5344–5386 (2006).
6. P. Lazzeretti, Ring currents. *Prog. Nucl. Mag. Res. Sp.* **36**, 1–88 (2000).
7. J. A. N. F. Gomes, R. B. Mallion, Aromaticity and ring currents. *Chem. Rev.* **101**, 1349–1383 (2001).
8. H. J. Dauben Jr., J. D. Wilson, J. L. Laity, Diamagnetic susceptibility exaltation in hydrocarbons. *J. Am. Chem. Soc.* **91**, 1991–1998 (1969).
9. D. Loss, P. Goldbart, Period and amplitude halving in mesoscopic rings with spin. *Phys. Rev. B* **43**, 13762–13765 (1991).
10. M. Mayor, C. Didschies, A giant conjugated molecular ring. *Angew. Chem. Int. Ed.* **42**, 3176–3179 (2003).
11. C. S. Wannere, P. von Ragué Schleyer, How aromatic are large  $(4n + 2)$   $\pi$  annulenes? *Org. Lett.* **5**, 865–868 (2003).
12. C. H. Choi, M. Kertesz, Bond length alternation and aromaticity in large annulenes. *J. Chem. Phys.* **108**, 6681–6688 (1998).
13. A. Soncini, P. W. Fowler, L. W. Jenneskens, Ring currents in large  $[4n + 2]$ -annulenes. *Phys. Chem. Chem. Phys.* **6**, 277–284 (2004).

14. T. Soya, W. Kim, D. Kim, A. Osuka, Stable [48]-, [50]-, and [52]dodecaphyrins(1.1.0.1.1.0.1.1.0.1.1.0): the largest Hückel aromatic molecules. *Chem. Eur. J.* **21**, 8341–8346 (2015).
15. N. Toriumi, A. Muranaka, E. Kayahara, S. Yamago, M. Uchiyama, In-plane aromaticity in cycloparaphenylene dications: a magnetic circular dichroism and theoretical study. *J. Am. Chem. Soc.* **137**, 82–85 (2015).
16. D. V. Kondratuk, L. M. A. Perdigão, A. M. S. Esmail, J. N. O'Shea, P. H. Beton, H. L. Anderson, Supramolecular nesting of cyclic polymers. *Nature Chem.* **7**, 317–322 (2015).
17. P. Liu, Y. Hisamune, M. D. Peeks, B. Odell, J. Q. Gong, L. M. Herz, H. L. Anderson, Synthesis of five-porphyrin nanorings by using ferrocene and corannulene templates. *Angew. Chem. Int. Ed.* **55**, 8358–8362 (2016).
18. J. K. Sprafke, D. V. Kondratuk, M. Wykes, A. L. Thompson, M. Hoffmann, R. Drevinskas, W.-H. Chen, C. K. Yong, J. Kärnbratt, J. E. Bullock, M. Malfois, M. R. Wasielewski, B. Albinsson, L. M. Herz, D. Zigmantas, D. Beljonne, H. L. Anderson, Belt-shaped  $\pi$ -systems: relating geometry to electronic structure in a six-porphyrin nanoring. *J. Am. Chem. Soc.* **133**, 17262–17273 (2011).
19. Z. Chen, C. S. Wannere, C. Corminboeuf, R. Puchta, P. von Ragué Schleyer, Nucleus-independent chemical shifts (NICS) as an aromaticity criterion. *Chem. Rev.* **105**, 3842–3888 (2005).
20. D. Geuenich, K. Hess, F. Kohler, R. Herges, Anisotropy of the induced current density (ACID), a general method to quantify and visualize electronic delocalization. *Chem. Rev.* **105**, 3758–3772 (2005).

21. N. G. Connelly, W. E. Geiger, Chemical redox agents for organometallic chemistry. *Chem. Rev.* **96**, 877–910 (1996).
22. G. Karunanithy, A. Cnossen, H. Müller, M. D. Peeks, N. H. Rees, T. D. W. Claridge, H. L. Anderson, A. J. Baldwin, Harnessing NMR relaxation interference effects to characterise supramolecular assemblies. *Chem. Commun.* **52**, 7450–7453 (2016).
23. E. I. Tellgren, T. Helgaker, A. Soncini, Non-perturbative magnetic phenomena in closed-shell paramagnetic molecules. *Phys. Chem. Chem. Phys.* **11**, 5489–5498 (2009).
24. R. Tamura, M. Ikuta, T. Hirahara, M. Tsukada, Positive magnetic susceptibility in polygonal nanotube tori. *Phys. Rev. B.* **71**, 045418 (2005).
25. Y. Yamamoto, Y. Hirata, M. Kodama, T. Yamaguchi, S. Matsukawa, K. Akiba, D. Hashizume, F. Iwasaki, A. Muranaka, M. Uchiyama, P. Chen, K. M. Kadish, N. Kobayashi, Synthesis, reactions, and electronic properties of 16  $\pi$ -electron octaisobutyltetraphenylporphyrin. *J. Am. Chem. Soc.* **132**, 12627–12638 (2010).
26. M. Gouterman, Spectra of porphyrins. *J. Mol. Spectrosc.* **6**, 138–163 (1961).
27. V. S.-Y. Lin, M. J. Therien, The role of porphyrin-to-porphyrin linkage topology in the extensive modulation of the absorptive and emissive properties of a series of ethynyl- and butadiynyl-bridged bis- and tris(porphinato)zinc chromophores. *Chem. Eur. J.* **1**, 645–651 (1995).
28. M. D. Peeks, P. Neuhaus, H. L. Anderson, Experimental and computational evaluation of the barrier to torsional rotation in a butadiyne-linked porphyrin dimer. *Phys. Chem. Chem. Phys.* **18**, 5264–5274 (2016).

29. A. Richards, University of Oxford Advanced Research Computing. *Zenodo* (2015), doi:10.5281/zenodo.22558.

**Supplementary Information** contains additional figures, tables, and methodological information. It is linked to the online version of the paper at [www.nature.com/nature](http://www.nature.com/nature)

**Acknowledgments** We thank the ERC (grant 320969), the EPSRC and the John Templeton Foundation for support, Dr. Barbara Odell for help with NMR spectroscopy and the Oxford Advanced Research Computing (ARC) centre for the high performance computing provision<sup>29</sup>. MDP thanks Exeter College, Oxford, for further support.

**Author contributions** MDP synthesised the compounds, performed the calculations, collected and analysed the spectroscopic data; TDWC assisted with NMR data collection and interpretation; HLA devised the project; MDP and HLA wrote the paper; all authors discussed the results and edited the manuscript.

**Author Information** Reprints and permissions information is available from [www.nature.com/reprints](http://www.nature.com/reprints). The authors declare no competing financial interests. Correspondence and requests for materials should be addressed to HLA ([harry.anderson@chem.ox.ac.uk](mailto:harry.anderson@chem.ox.ac.uk)).

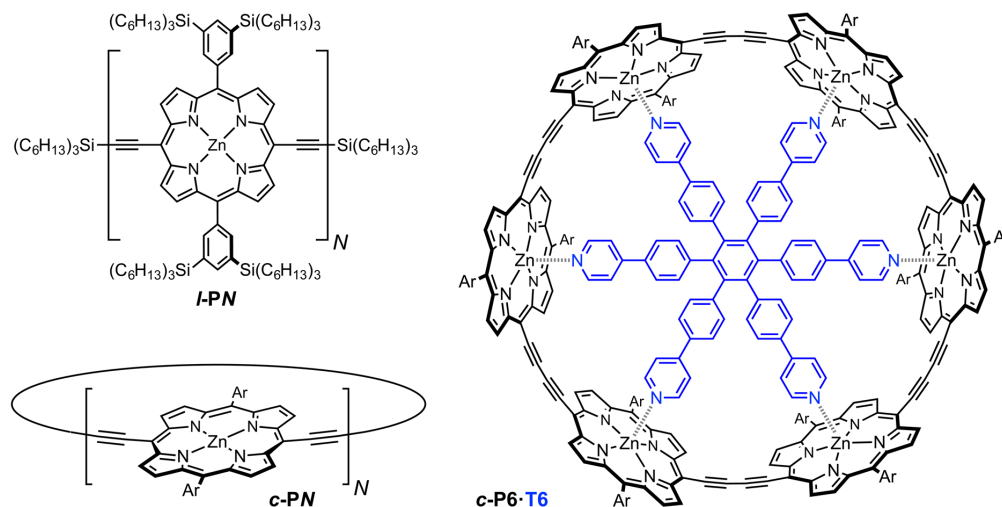


**Fig. 1. Molecular structures of the butadiyne-linked porphyrin oligomers used in this study: *I*-PN, *c*-PN and *c*-P6·T6.** Ar = (3,5-bis(trihexylsilyl))phenyl as shown for *I*-PN.

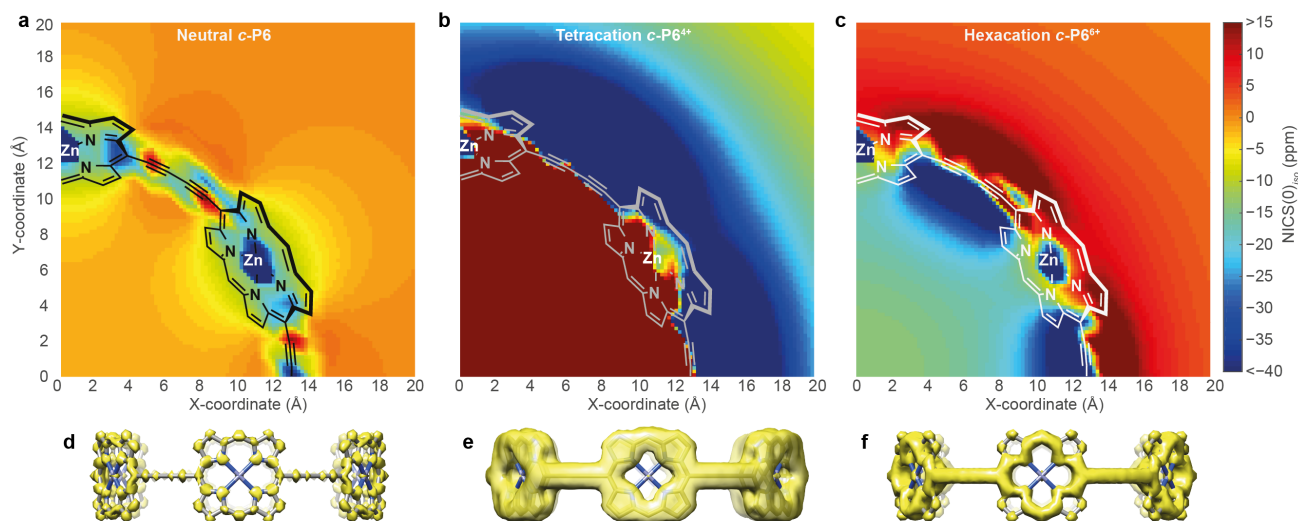


**Fig. 2. Summary of computational results.** NICS(0)<sub>iso</sub> grids in the xy plane of (a) *c*-P6, (b) *c*-P6<sup>4+</sup> and (c) *c*-P6<sup>6+</sup>. The colour axis has been truncated to compare data for all three oxidation states on the same scale. See SI Figure S8 for grids with individual scales. (d), (e) and (f) show corresponding ACID plots for each oxidation state. The yellow iso-surface depicts the anisotropy of the induced current density, plotted with an isovalue of 0.1 a.u.

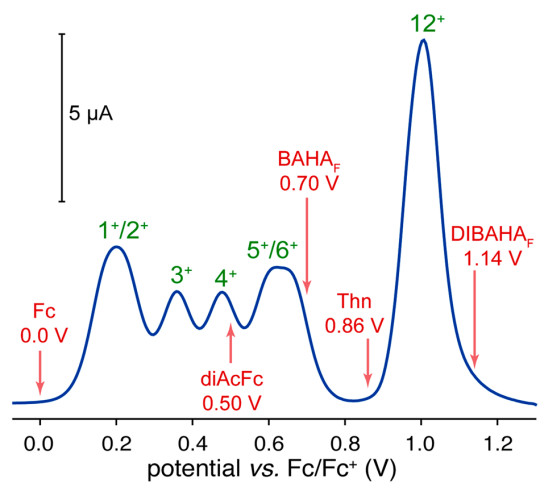


**Fig. 3. Square-wave voltammetry** of *c*-**P6·T6** in CH<sub>2</sub>Cl<sub>2</sub> (0.1 M Bu<sub>4</sub>NPF<sub>6</sub>). The red arrows show the first reduction potential of each oxidant<sup>21</sup>; abbreviations are defined in the text.

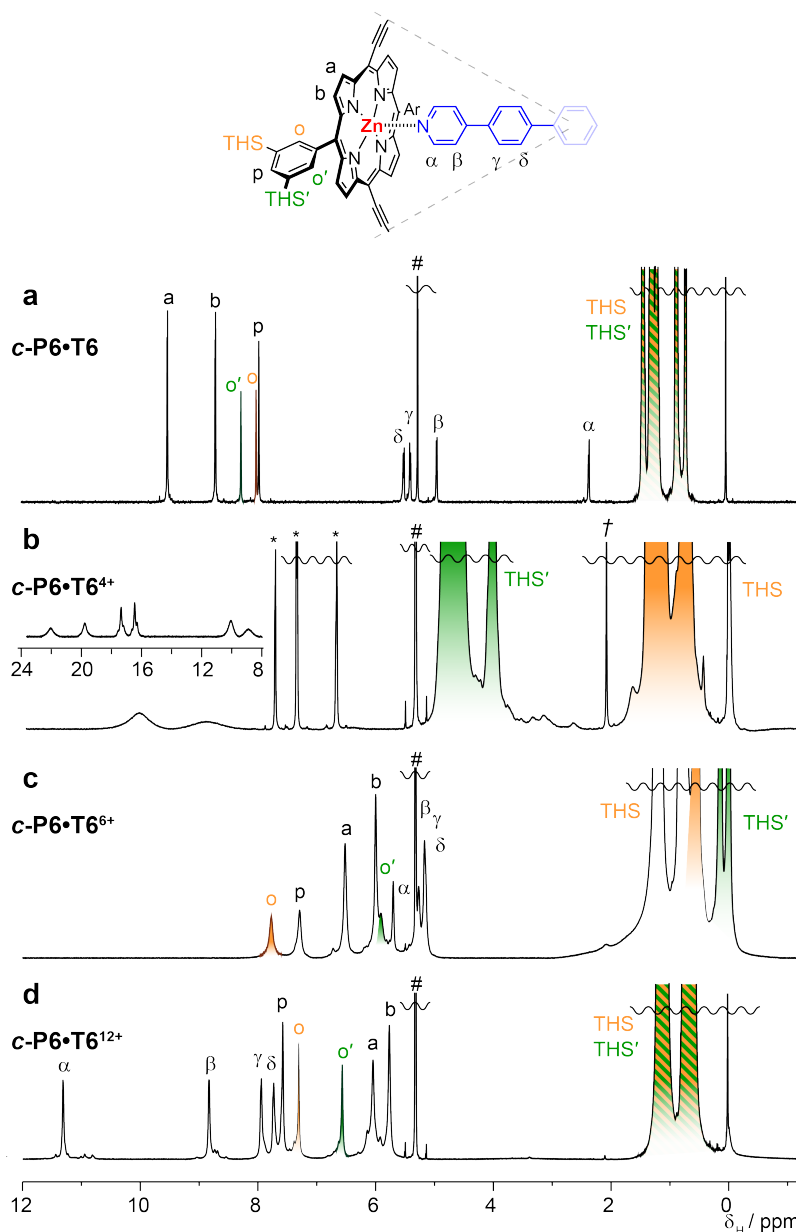


**Fig. 4.**  $^1\text{H}$  NMR spectra (500 MHz,  $\text{CD}_2\text{Cl}_2$ ) of (a) neutral  $c\text{-P6}\cdot\text{T6}$  (298 K); (b)  $c\text{-P6}\cdot\text{T6}^{4+}$  generated by titration with  $\text{DIBAHA}_\text{F}$ , 223 K; (c)  $c\text{-P6}\cdot\text{T6}^{6+}$  generated during titration with  $\text{AgSbF}_6/\text{I}_2$ , 223 K; (d)  $c\text{-P6}\cdot\text{T6}^{12+}$  generated by oxidation with excess  $\text{DIBAHA}_\text{F}$ , 223 K. The inset molecular structure shows the symmetric unit of the 6-fold symmetric  $c\text{-P6}\cdot\text{T6}$ . The peaks labelled # and \* arise from  $\text{CHDCl}_2$  and neutral oxidant (tris(2,4-dibromophenyl)amine), respectively. Unlabelled resonances are not assigned. † is an unknown impurity. The full spectra, without truncated peaks, are shown in SI Fig. S27.

## **Supplementary Materials:**

Materials and Methods

Figures S1–S26

Tables S1–S5

Datasets: Computational data (calculated Cartesian coordinates and energies for neutral ***c*-P6**, ***c*-P6<sup>4+</sup>**, ***c*-P6<sup>6+</sup>** and ***c*-P6<sup>12+</sup>**).

## **Affiliation:**

University of Oxford, Department of Chemistry, Chemistry Research Laboratory, Oxford OX1  
3TA United Kingdom

\*Correspondence to: [harry.anderson@chem.ox.ac.uk](mailto:harry.anderson@chem.ox.ac.uk).